Journal of
Medicinal Chemistry

Article

Bioisosteric Replacement of Arylamide-linked Spine Residues by N-Acylhydrazones and Selenophenes as Design Strategy to Novel Dibenzosuberone Derivatives as Type I½ p38# MAP Kinase Inhibitors

Júlia Galvez Bulhões Pedreira, Philipp Nahidino, Mark Kudolo, Tatu Pantsar, Benedict-Tilman Berger, Michael Forster, Stefan Knapp, Stefan A. Laufer, and Eliezer J. Barreiro

J. Med. Chem., **Just Accepted Manuscript** • DOI: 10.1021/acs.jmedchem.0c00508 • Publication Date (Web): 28 May 2020

Just Accepted

is published by the American Chemical Society. 1155 Sixteenth Street N.W., Washington, DC 20036

Bioisosteric Replacement of Arylamide-linked Spine Residues by *N*-Acylhydrazones and Selenophenes as Design Strategy to Novel Dibenzosuberone Derivatives as Type I½ p38α MAP Kinase Inhibitors

Júlia G. B. Pedreira[a,b], Philipp Nahidino[c], Mark Kudolo[c], Tatu Pantsar,[c,d], Benedict-Tilman Berger,[e,f], Michael Forster[c], Stefan Knapp,[e,f], Stefan Laufer[c,g,h], Eliezer J. Barreiro[a,b]

[a]Laboratory of Evaluation and Synthesis of Bioactive Substances (LASSBio), Federal University of Rio de Janeiro (UFRJ), 21944-971, Rio de Janeiro, RJ, Brazil.

[b]Graduate Program of Chemistry (PGQu), Chemistry Institute, UFRJ, 21941-909, Rio de Janeiro, RJ, Brazil.

[c]Department of Pharmaceutical and Medicinal Chemistry, Institute of Pharmaceutical Sciences, Eberhard Karls Universität, Tübingen, Auf der Morgenstelle 8, 72076 Tübingen, Germany.

[d]School of Pharmacy, University of Eastern Finland, Yliopistonranta 1, 70210 Kuopio, Finland.

[e]Institute for Pharmaceutical Chemistry, Johann Wolfgang Goethe-University, Max-von-Laue-Str. 9, D-60438 Frankfurt am Main, Germany

[f]Structural Genomics Consortium (SGC), Buchman Institute for Life Sciences, Johann Wolfgang Goethe-University, Max-von-Laue-Str. 15, D-60438 Frankfurt am Main, Germany

[g]Cluster of Excellence iFIT (EXC 2180) "Image-Guided and Functionally Instructed Tumor Therapies", University of Tübingen, 72076 Tübingen, Germany

[h]Tübingen Center for Academic Drug Discovery & Development (TüCAD2), 72076 Tübingen, Germany

ABSTRACT: The recent disclosure of type I½ inhibitors for p38α MAPK demonstrated how the stabilization of the R-spine can be used as a strategy to greatly increase the target residence time (TRT) of inhibitors. Herein, we describe first time *N*-acylhydrazone and selenophene residues as spine-motives, yielding metabolically stable inhibitors with high potency on enzymatic, NanoBRET and whole blood assays, improved metabolic stability and prolonged TRT.

INTRODUCTION

Almost 20 years ago, with the elucidation of the kinome, protein kinases have become one of the most actively studied pharmacological targets.[1] The potential for modulating the often increased activity of such proteins in the treatment of various pathologies has become increasingly attractive as a new therapeutic approach. [2,3] One of the most studied protein kinases is the p38 Mitogen-activated protein kinase (MAPK). This protein is activated upon cellular stress and it regulates biosynthesis of various proinflammatory cytokines. Of the four isoforms of p38 (α, β, γ and δ), the p38α is the only isoform that is ubiquitously expressed in all tissues and has been associated with tumor development upon deregulation of expression levels. Therefore, p38α is considered an attractive target for cancer treatment.[4] Eli Lilly's compound, LY2228820, is the most recent example to reach phase II clinical trials for treatment of ovarian cancer.[5] Despite major efforts to target this protein, still no p38α MAPK inhibitors have been approved by the FDA, which is most likely due to off-target toxicity and lack of efficacy *in vivo*.[6,7]

Skepinone-L (**1**, Figure 1A) was one of the first highly selective p38α inhibitors developed. It is very potent, displaying an IC_{50} of 5 nM and no relevant off-target activity up to 1 μM within a panel of 402 kinases.[8,9] It is ATP-competitive, and classified as type I inhibitor. The crystal structure of **1** in complex with p38α reveals an unique hinge-interaction via a so called glycine flip with the dibenzosuberone scaffold (PDB ID: 3QUE).[8] The induction of this glycine flip enables the great improvement of selectivity compared to other p38α MAPK inhibitors. [10,11]

Many efforts were made to subsequently develop optimized inhibitors from **1**, which led to the identification of compounds **2** and **3** (Figure 1B-D). Both also displayed an exceptional potency in enzymatic assays ($IC_{50} < 3$ nM), together with an outstanding selectivity within a broad panel of kinases.[12–14] These compounds, although initially designed as type II inhibitors, showed an atypical binding mode in the p38α MAPK. The crystal structure (PDB ID: 5TCO) revealed an edge-to-face interaction between the aromatic residues of the eastern amide and Phe169 of the DFG motif (Figure 1C), inducing a DFG-in conformation typically seen with type I inhibitors. This interaction involves an important regulatory

structural element, the regulatory spine (R-spine), which is assembled upon kinase activation.[15] This spine is formed by Leu86, Leu75, Phe169 and His148. Thus, compounds **2** and **3** appeared to stabilize the R-spine and induce an active-like conformation of the kinase. For their capacity to combine type I and II interactions, these inhibitors were named as type I½.

In earlier studies we demonstrated that these interactions and stabilization of the R-spine greatly influences the inhibitor's target residence time (TRT).[14] While **1** has a relatively short TRT of 88 s, inhibitor **2** has a slightly prolonged TRT of 184s and finally **3** shows a substantial increase to 746 s. The latter represents a difference of one order of magnitude compared to **1**, and this improvement is directly related to the R-spine stabilization. The increase in TRT observed from **2** to **3** was attributed to the significantly higher electron density of the thiophene compared to phenyl residue, which resulted in a stronger interaction with the Phe169 residue. Optimization of the TRT evolved to a promising design concept in medicinal chemistry over the last years, since it is supposed to bring along several advantages such as improved PK, increased *in vivo* efficacy, and reduced adverse effects.[16] Compounds **2** and **3**, however, suffer from metabolic instability. *In vitro* studies demonstrated that these compounds undergo metabolic degradation, especially via eastern amide hydrolysis, resulting in a loss of the R-spine interacting residue. This is a challenge to overcome in order to advance through the later development stages and maintain efficacy *in vivo*.

The combination of all the distinctive interaction opportunities in the p38α MAPK is a promising and interesting feature for the development of new inhibitors that are eligible to proceed in the drug development process, since it may provide improved selectivity and increased efficacy *in vitro* and *in vivo*. In this work, we focus on the design of new dibenzosuberone compounds by a bioisosteric replacement at the R-spine interacting residue, with the aim to maintain the excellent potency of the underlying compound class, together with improved target residence time and metabolic stability.

Structure Based Design. With the lead structures **2** and **3** as starting points, our initial design approach was to introduce a new and metabolically stable functional group to replace the amide, that could also be suitable for interactions with the R-spine (Figure 1D). As the dibenzosuberone scaffold is crucial to induce the glycine flip in the hinge, we kept it unchanged as a main building block. We also opted to maintain the morpholinoethyl-amide substitution to occupy HRII, since it was known from previous SAR studies that it displays a well-balanced profile acting as a solubilizing group.[13]

As an alternative for the eastern amide, we proposed the *N*-acylhydrazone (NAH) group combined with the same set of R-spine interacting residues as prototypes **2** and **3**, resulting

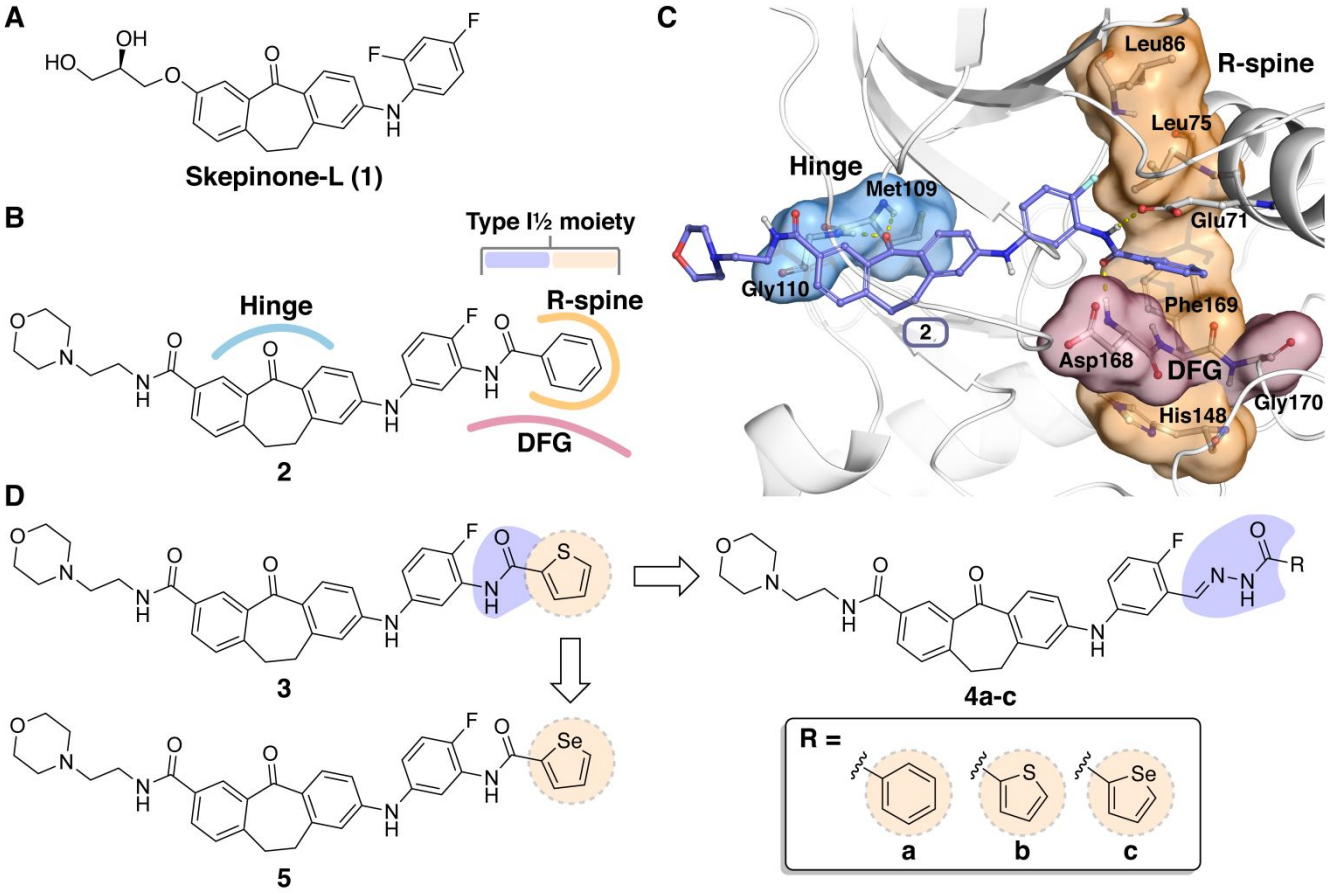

Figure 1. (**A**) Chemical structure of Skepinone-L (**1**). (**B**) Chemical structure of **2**. Type I ½ inhibitors contain an additional R-spine interacting moiety. (**C**) Crystal structure of compound **2** in complex with p38α MAPK (PDB ID: 5TCO). Highlighted are the R-spine (orange), DFG residues Asp168 and Gly170 (red) and dibenzosuberone interacting residues Met109 and Gly110 from the hinge region (blue), notice the glycine-flip of Gly110. The type I½ R-spine interacting moiety displays an edge-to-face π-π interaction with Phe169. The amide forms H-bonds to the side chain of Glu71 and to the backbone of Asp168 of the DFG motif (**D**) Schematic representation of the structural design of the new *N*-acylhydrazone derivatives **4a-b** and selenophene isosters **4c** and **5**.

in the corresponding inhibitors **4a** and **4b** (Figure 1D). This bioisosteric replacement was proposed to be able to maintain key interactions in the HRI, and also target the DFG motif for the R-spine stabilization.

Additionally, the amide replacement was supposed to be advantageous for the metabolic profile, since NAHs have been previously described as being more stable than amides, and do not undergo cleavage as easily. [17,18] Finally, as a strategy to explore specifically the R-spine interaction, we also designed two additional compounds based on the isosteric substitution of thiophene for selenophene (**4c** and **5**). As the electronic density of the selenophene ring is different from its O- or S-isomers, the design of organo-selenium compounds has recently attracted attention as a strategy to explore new type of interactions with a target-protein.[19–22] In the same way as the electronegativity decreases within the group of chalcogenes (O >> S > Se), the electronic density of the corresponding five-membered heterocycles increases from furan to thiophene to selenophene. In this regard, our hypothesis was that this is supposed to positively affect the interaction with Phe169 and therefore increase the TRT via an enhanced stabilization of the R-spine.

RESULTS AND DISCUSSION

Chemistry. The synthesis of the new dibenzosuberone derivatives started with the preparation of the aniline linkers, as described in Scheme 1. Intermediate **8** was synthetized by bis protection of the amino group in 2-fluoro-5-nitroaniline (**6**) with di-*tert*-butyl dicarbonate (Boc_2O) followed by reduction of the nitro group in **7** with Pd/C under hydrogen atmosphere. For the preparation of intermediate **11**, 2-fluoro-5-nitrobenzaldehyde (**9**) was acetal-protected in MeOH with dimethoxypropane, followed by subsequent reduction of nitro group with hydrogen on Pd/C.

Both aniline derivatives **8** and **11** were coupled via a Buchwald-Hartwig amination with key intermediate **12** (see Supplementary)[14] using standard cross-coupling conditions, to afford either **13** or **14** (Scheme 2). For the preparation of the NAHs, intermediate **13** was submitted to a one-pot deprotection and condensation sequence with the corresponding hydrazides **28**, **29** or **32** (SI) to afford the desired final compounds **4a-c**.

To prepare the amide **5**, intermediate **14** was first deprotected with TFA to yield the aniline **15** followed by standard amide coupling via the acid chloride derived by the activation of the carboxylic acid **31** (SI).

Biological evaluation. The *N*-acylhydrazone derivatives (**4a** and **4b**), along with the selenophene isosters (**4c** and **5**), were initially tested in an ADP-glo assay[23] to determine inhibitory activity for p38α MAPK (Table 1). In this initial screening, all compounds displayed low nanomolar activity. Since the measured IC_{50} values are ranging near the lower detection limit of this assay system, it is difficult to derive proper structure-activity relationships based on this data between these substituents. Nonetheless, the inhibition profile primarily demonstrates that introduction of the NAH moiety (compounds **4a-c**) and the isosteric substitution in the aromatic system maintains the potency for the enzyme inhibition, compared to prototypes **2** and **3**.

Scheme 1: Synthetic route for preparation of aniline intermediate 8 and 11[a].

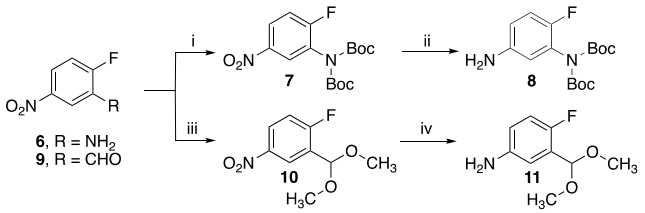

[a]Reagents and reaction conditions: (i) Boc_2O, $DMAP_{cat}$, TEA, THF, r.t., 47%; (ii) H_2, Pd/C, MeOH, r.t., 59%; (iii) dimethoxypropane, TsOH, MeOH, r.t., 85%; (iv) H_2, Pd/C, EtOAc, r.t., 95%.

After these promising results, the compounds were evaluated in a cellular environment using a NanoBRET assay (Table 1). Cellular evaluation is an important step to verify compound permeability and whether they maintain the activity observed at the isolated protein in a much more dynamic system where cellular concentrations of the competitive substrate ATP are present. Overall, a good agreement between the enzymatic and the cellular data was proven with low nanomolar IC_{50} values, demonstrating a good cell permeability and cellular target engagement.

Subsequently, we assessed the activity in a human whole-blood TNF-α assay (Table 1). This test system represents a reliable model for more complex biological environments, where factors such as solubility, cell-cell-interaction and others, influence the compounds activity and efficacy.[24] Within the NAH series, the TNF-α assay revealed a significant loss of potency from phenyl (**4a**), to the thiophene (**4b**), and to the selenophene (**4c**) substituent.

Scheme 2. Preparation of the dibenzosuberone derivatives **4a-c** and **5**[a]

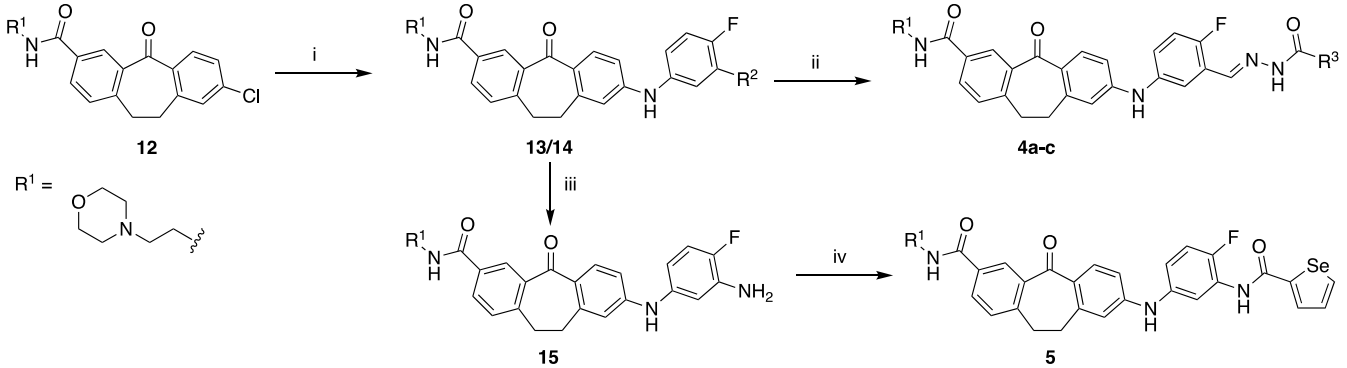

[a]Reagents and conditions: (i) **8** or **11**, K_2CO_3, BrettPhos Pd G3, 1,4-dioxane, 90˚C, 87 – 93%; (ii) (1) H_2SO_4, EtOH, r.t., (2) ArN_2H_4, EtOH, room temperature 75 – 95%; (iii) TFA, DCM, r.t., 54%; (iv) (1) **31**, oxalyl chloride, DMF, THF, (2) acid chloride, Et_3N, THF, 0˚C, 46%.

Table 1: Biological data of the Dibenzosuberone derivatives.

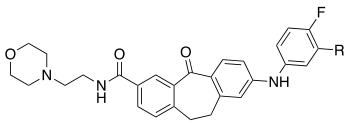

	R	ADP-Glo [nM][a]	NanoBRET [nM][b]	TNFα [nM][c]	TRT [s][d]
4a	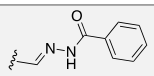	19.7	6.3 ± 1.1	47 ± 13	830 ± 146
4b	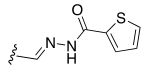	29.7	15.5 ± 1.2	276 ± 66	1341 ± 222
4c	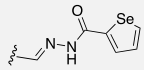	16	30.4 ± 1.2	490 ± 168	1013 ± 146
5	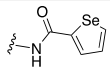	24.6	4.9 ± 1.2	101 ± 35	1596 ± 22[e]
2	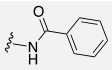	4	4.3 ± 2.0	38 ± 1.1	184 ± 37[e]
3	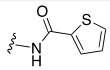	12	N.D.	43 ± 0.8	746[f]

[a]results from an activity-based ADP-Glo assay (Promega); [b]results from a cellular reporter-displacement NanoBRET assay (Promega); [c]results from a human whole blood TNF-α release assay; [d]results from a time-resolved FRET assay; [e]measurement from duplicate; [f]single measurement; N.D. = not determined

This may be attributed to solubility issues or differences in plasma protein binding, given that thiophene and selenophene are more lipophilic when compared to phenyl. Nevertheless, the NAH phenyl derivative **4a** displays a good activity, with an IC_{50} value of 47 nM, which is comparable to its corresponding amide analogue **2** with an IC_{50} value of 38 nM (determined from previous studies).[13] For the selenophene-substituted amide **5**, we also observed a 2-fold loss of potency when compared to amide analogues **2** or **3**, but again this is most probably correlated with the higher lipophilicity as already discussed for the NAHs.

Putative binding mode of *N*-acylhydrazones. To ascertain the putative binding mode of the NAH-derived compounds, which contain substantially longer type I½ R-spine interacting moieties compared to previously reported inhibitors, we utilized *in silico* methods (see details in SI). Perhaps unsurprisingly, docking approaches with Glide and Induced fit docking (IFD)[25], which allows a limited movement of the protein, resulted only in reasonable poses for derivatives with smaller residues than the here shown aromatic rings (Figure S2). To evaluate if this type of binding mode could be realistic with compounds that are carrying considerably larger substituents, we conducted extensive molecular dynamics (MD) simulations with **4a** and **4b** (aggregate of 21.6 µs) starting from a similar binding conformation as observed in the aforementioned docking studies. Indeed, in all of the simulations with these bulkier R-spine interacting NAHs we observed stable binding (Figure. 2; Figures. S3-9; Supplementary movies). The interaction to Met109 of the hinge appears extremely stable throughout the simulations (Figures S7 and S9). R-spine interacting moieties displayed sufficiently stable interactions and contacts to Phe169 and Leu75. The iminic nitrogen atom in the NAH displays water mediated interactions to Asp168 (or Lys53). In comparison to the crystal

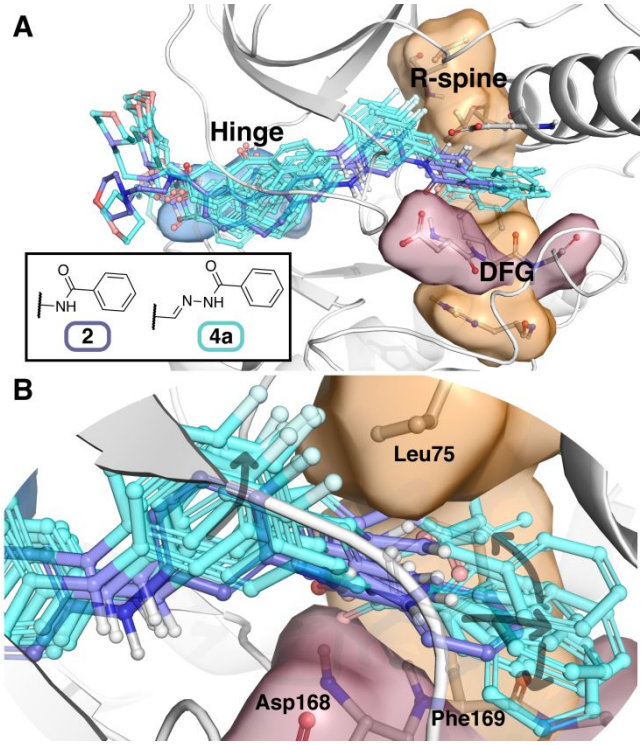

Figure 2: Putative binding mode of NAHs. (**A**) Representative snapshots from MD simulations of **4a** (cyan) aligned with crystal structure of **2** (blue) (PDB ID: 5TCO). The main differences compared to compound **2** are zoomed in (**B**). The fluorophenyl moiety orientation of **4a** is shifted deeper into the protein (single black arrow). Moreover, type I ½ moiety of **4a** is oriented deeper into the pocket and capable of adapting different conformations in the R-spine interacting region (black arrows).

structure of the corresponding shorter phenylamide containing compound **2**, the NAHs display a shift in the binding orientation of the middle fluorophenyl group deeper into the protein in a way that the type I½ residue is able to accommodate proper binding and interactions with the R-spine residues (Fig. S3; Fig. S8; Supplementary movies).

Determination of Target Residence Time (TRT). The set of biological assays confirmed that the conducted structural modifications did not compromise the potency of the dibenzosuberone derivatives. Additionally, MD simulations suggested that the NAH moiety could fit into the active pocket and possibly uphold the key interactions with the protein. In order to better correlate the data and to investigate the impact of the different aromatic residues in the overall biological profile of our compounds, we determined the TRT on the p38α MAPK using a TR-FRET-based method (Table 1).

Interestingly, the NAH moiety appears to provide a significant increase in the TRT. Comparison between specific aromatic residues shows, that there was an increase of almost 5-fold between **2** and **4a**, and almost 2-fold between **3** and **4b**. However, the same is not observed for the selenophene pair **4c** and **5**, as the NAH derivative displays slightly decreased TRT, which is possibly correlated to conformational constraints of this fragment due to intramolecular chalcogen interactions (see Supplementary).[26–28] Nonetheless, MD simulations suggest that NAH compounds reach deeper into the hydrophobic area within the R-spine region and display additional water mediated interactions from the imine nitrogen atom. These additional interactions may play a decisive role in the increased TRT.

Also, in agreement with our hypothesis, substitution in the amide for the selenophene isoster (**5**) revealed a great increase of TRT compared to its prototypes **2** and **3**. This is most probably due to an ability of the selenophene ring to make a stronger π–π interaction with the Phe169 residue

***In vitro* metabolism.** Considering the good overall biological profile obtained for derivative **4a**, combined with a prolonged TRT, we selected this compound to be evaluated for its metabolic stability. Additionally, we included compound **5** to obtain a more detailed insight into the biotransformation profile of this isoster. There are only sparse descriptions of metabolic stability of seleno-aromatic compounds, but from comparison to thiophene, it may be expected to proceed via oxidation of the ring, which is known to have great implications on the toxicity of thiophene-containing bioactive compounds.[29] Selenium, however, has a lower redox potential, so that oxidation reactions in a biological system could differ substantially when compared from sulfur.[30,31] To investigate the metabolic stability of the chosen compounds, the experiments were performed with human liver microsomes (HLM).

After 180 minutes of incubation, there was no significant formation of metabolites from the NAH derivative **4a** (Figure 3). This corroborates with the hypothesis that the NAH functional group is more stable than an amide and appears not to undergo hydrolysis in this model of the first phase of metabolism. For compound **5** we observed a more prominent degradation with only 43% of the parent compound remaining after the full incubation time. The major metabolite could be identified with m/z of 489. This equals the mass of the amide hydrolysis metabolite, as previously observed for compounds **2** and **3**. Other species formed from incubation could not be identified as common metabolites, and might originate from fragmentation during the analysis. Nevertheless, there was no evidence of oxidation in the selenophene moiety.

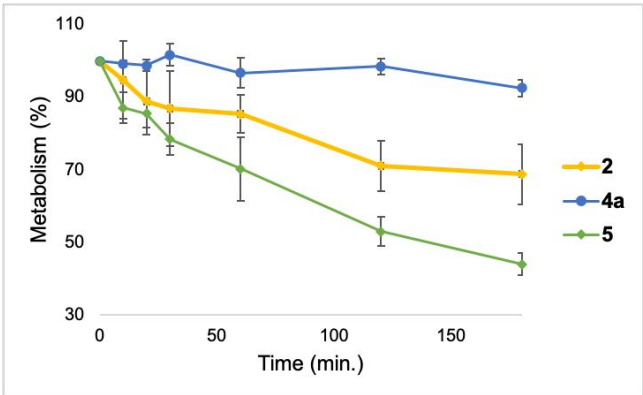

Figure 3. *In vitro* metabolism of selected compounds. Graphical representation of analyte decrease over 180 minutes in incubation with HLM.

CONCLUSION

We were able to synthetize new *N*-acylhydrazone derivatives of the dibenzosuberone p38α MAPK inhibitor series, with low nanomolar activity and good metabolic stability. From a series of assays of increasing levels of biological complexity, we identified compound **4a**, that displayed good biological profile, with metabolic stability in microsomal studies, combined with an increased TRT compared to its prototype **2**.

From the set of inhibitors, we demonstrated that isosteric replacement of sulfur to selenium does not affect the potency of inhibition at the enzyme. Moreover, based on TRT measurements we observed a more than 2-fold increase of the selenophene isoster **5** compared to its thiophene analogue **3**, suggesting that this new residue is able to further stabilize the spine by a π–π interaction with the Phe169. This work demonstrates that the isosteric replacement is a valid strategy to explore a new chemical space in drug discovery that could improve target interaction. We believe that the bioisosteric approach described in this study could ultimately be an useful tool for Medicinal Chemistry research.

EXPERIMENTAL SECTION

Chemistry. All starting materials, reagents and (anhydrous) solvents were commercially available and were used without further purification. ^{1}H and ^{13}C NMR spectra were obtained with Bruker Avance 200 or Bruker Avance 400 spectrometer. The spectra were calibrated against the residual proton peak of the used deuterated solvent. Chemical shifts (δ) are reported in parts per million. Mass spectra were obtained by Advion DC-MS (ESI) and from the MASS Spectrometry Department (FAB-MS; ESI-HRMS), Institute of Organic Chemistry, Eberhard-Karls-Universität Tübingen. HPLC analysis was carried out on an Agilent 1100 Series LC with Phenomenex Luna C8 column (150 x 4.6 mm, 5 µm) and detection was performed with a UV DAD at 254 nm and 230 nm wavelength. Elution was carried out with the following gradient: 0.01 M KH_2PO_4, pH 2.30 (solvent A), MeOH (solvent B), 40 % B to 85 % B in 8 min, 85 % B for 5 min, 85 % to 40 % B in 1 min, 40 % B for 2 min, stop time 16 min, flow 1.5 ml/min. Thin-layer-chromatography (TLC) analyses were performed on fluorescent silica gel 60 F254 plates (Merck) and visualized under UV illumination at 254 and 366 nm. Column chromatography was performed on Davisil LC60A 20−45 µm silica from Grace Davison and Geduran Si60 63−200 µm silica from Merck for the precolumn using an Interchim PuriFlash 430 automated flash chromatography system. All synthesized final compounds had purity of at least 95% as determined by HPLC at two different wavelengths (230 nm / 254 nm).

The representative preparation of compound **4a** is given here. All other final compounds were synthesized following similar procedures and detailed descriptions and analytic can be found in the SI.

*2-(Dimethoxymethyl)-1-fluoro-4-nitrobenzene (**10**)* A volume of 545 µL of 2,2-dimethoxypropane (4.44 mmol, 1.5 eq.) and a catalytic amount of *p*-toluenesulfonic acid (0.05 g, 0.29 mmol, 0.1 eq.) were added to a solution of the aldehyde (**9**) (0.5 g, 2.95 mmol, 1 eq.) in absolute methanol (10 mL) and stirred overnight at room temperature. The reaction mixture was then poured into 30 mL of saturated K_2CO_3 aqueous solution and extracted using dichloromethane. The organic extracts were dried using Na_2SO_4, filtrated and concentrated under reduced pressure. The crude product was purified on flash chromatography (0-30% EtOAc/PE) to obtain **10** as a transparent oil. Yield: 545 mg (2.53 mmol, 85%); ^{1}H NMR (400 MHz, $CDCl_3$): δ 8.51 (dd, 1H), 8.25 (m, 1H), 7.21 (t, 1H), 5.63 (s, 1H), 3.39 (s, 6H). ^{13}C NMR (100 MHz, $CDCl_3$) δ (ppm): 162.5, 144.3, 127.4, 126.2, 124.9, 116.7, 97.5, 53.8.

*3-(Dimethoxymethyl)-4-fluoroaniline (**11**)* Intermediate **10** (0.54 g, 2.53 mmol) was dissolved in EtOAc (10 mL) and 10 wt % of palladium on activated carbon was added. The reaction was stirred at room temperature for 4 hours under hydrogen atmosphere. Afterwards, the reaction mixture was filtered over Celite® and the solvent removed under pressure to afford **11** as a brown oil. Yield 465 mg (2.51 mmol, 98%); ^{1}H NMR (400 MHz, $CDCl_3$): δ 6.87–6.82 (m, 2H), 6.62–6.58 (m, 1H), 5.53 (s, 1H), 3.56 (s, 2H), 3.38 (s, 6H). ^{13}C NMR (100 MHz, $CDCl_3$) δ (ppm): 168.4, 142.5, 125.0, 116.5, 115.9, 114.0, 98.8, 53.8.

*8-((3-(Dimethoxymethyl)-4-fluorophenyl)amino)-N-(2-morpholinoethyl)-5-oxo-10,11-dihydro-5H-dibenzo[a,d][7]annulene-3-carboxamide (**13**)* The dibenzosuberone intermediate (**12**, 0.5 g, 1.25 mmol, 1 eq.), aniline **11** (278 mg, 1.50 mmol, 1.2 eq.) and K_2CO_3 (519 mg, 3.76 mmol, 3 eq.), were suspended in dry dioxane (10 mL) in a Schlenck flask. The mixture was degassed and backfilled with argon three times. BrettPhos Pd G3 precatalyst (45 mg, 0.05 mmol, 0.04 eq) was added and the degassing procedure was repeated. The reaction was heated to 90˚C and stirred for 4h. After cooling, the reaction was quenched with a saturated solution of NH_4Cl and then extracted with DCM. The organic layer was dried over Na_2SO_4 and evaporated in a rotary evaporator. The crude product was purified using flash chromatography (0 - 8% MeOH/DCM) to obtain **13** as a yellow solid. Yield 600 mg (1.09 mmol, 87%); ^{1}H NMR (400 MHz, $CDCl_3$) δ 8.13 (d, 1H), 7.93 (dd, 1H), 7.69 (dd, 1H), 7.31-7.26 (m, 3H), 7.06-7.04 (m, 1H), 6.93 (t, 1H), 6.88 (bs, 1H), 6.78-6.74 (m, 1H), 5.53 (s, 1H), 5.43 (s, 1H), 3.74 (t, 4H), 3.56 (q, 2H), 3.36 (s, 6H), 3.21-3.09 (m, 4H), 2.62 (bs, 2H), 2.60 (bs, 4H). ^{13}C NMR (100 MHz, $CDCl_3$) δ 196.4, 166.6, 154.1, 144.4, 141.3, 140.5, 140.4, 140.2, 139.6, 133.5, 133.3, 131.3, 129.5, 127.5, 127.4, 125.3, 125.1, 119.0, 117.0, 116.4, 98.8, 67.0, 57.0, 36.3, 33.6, 28.8.

*8-((3-((2-Benzoylhydrazineylidene)methyl)-4-fluorophenyl)amino)-N-(2-morpholinoethyl)-5-oxo-10,11-dihydro-5H-dibenzo[a,d][7]annulene-3-carboxamide (**4a**).* The acetal intermediate (**13**, 0.1 g, 0.18 mmol) was solubilized in EtOH (5 mL) and a 250 µL of H_2SO_4 was added. The reaction mixture was stirred at room temperature for 30 min, and then the corresponding hydrazide was added (25 mg, 1 eq.). Stirring was maintained at room temperature for 4 h. The solvent was then removed under pressure and the product was precipitated by addition of water in an ice bath. The precipitate was filtrated under vacuum and crude product was purified using flash chromatography (0 - 5% MeOH/DCM) to afford the NAH compound **4a** at 89% yield as a yellow solid (0.1 g). ^{1}H NMR (400 MHz, $CDCl_3$) δ 10.79 (s, 1H), 8.50 (s, 1H), 8.32 (s, 1H), 8.03 (d, 1H), 7.96 (d, 2H), 7.88 (d, 1H), 7.59 (bs, 1H), 7.54–7.50 (m, 1H), 7.42 (t, 2H), 7.29 (s, 1H), 7.17-7.15 (m, 2H), 6.90 (t, 1H), 6.81 (d, 1H), 6.73 (s, 1H), 6.63 (s, 1H), 3.75-3.73 (t, 4H), 3.61-3.59 (q, 2H), 2.99-2.96 (m, 4H), 2.69-2.67 (m, 2H), 2.66-2.57 (bs, 4H).^{13}C NMR (100 MHz, $CDCl_3$) δ**:** 191.3, 167.2, 165.1, 156.3, 148.5, 145.7, 145.3, 141.4, 140.2, 139.9, 139.2, 137.2, 134.3, 133.0, 132.8, 132.5, 131.2, 129.3, 129.0, 128.8, 127.8, 124.3, 119.4, 116.6, 114.9, 113.0, 66.8, 57.3, 53.5, 36.4, 35.93, 34.7. HPLC: 6.127 min (96,05 %). ESI-HRMS $[M+H]^+$ calculated: 620.26676, found: 620,266687.

ASSOCIATED CONTENT

Supporting Information

Additional experimental details for preparation of the compounds; ^{1}H NMR, ^{13}C NMR, HR-MS, HPLC molecular modelling, MD simulations, and biological assays. The supplementary movies and full-length raw trajectories are freely available at https://doi.org/10.5281/zenodo.3696749. Molecular formula strings (CSV) file available.

AUTHOR INFORMATION

Corresponding Author

Dr. Stefan Laufer: Phone + 49 7071 2972459 Email: stefan.laufer@uni-tuebingen.de
Dr. Eliezer J. Barreiro: Phone +55 21 25626644 E-mail addresses: ejbarreiro@ccsdecania.ufrj.br, ejbarreiro@gmail.com Both corresponding authors contributed equally (shared)

Funding Sources

The authors would like to thank CAPES/INCT-INOFAR (Project No 88887.3182253/2019-00), DAAD (Project. No. 5749963) and the Baden-Württembergisches Brasilien-Zentrum from the University of Tübingen for funding of this project. S.L. and iFIT are funded by the Deutsche Forschungsgemeinschaft (DFG, German Research Foundation) under Germany's Excellence Strategy - EXC 2180 – 390900677. TüCAD2 is funded by the Federal Ministry of Education and Research (BMBF) and the Baden-Württemberg Ministry of Science as part of the Excellence Strategy of the German Federal and State Governments. T.P. acknowledges the Orion Research Foundation sr for financial support and funding from the European Union's Horizon 2020 research and innovation programme under the Marie Sklodowska-Curie grant agreement No 839230. SK and B-TB are grateful for support by the German cancer network DKTK, the Frankfurt Cancer Centre (FCI) as well as the SGC, a registered charity that receives funds from AbbVie, Bayer Pharma AG, Boehringer Ingelheim, Canada Foundation for Innovation, Eshelman Institute for Innovation, Genome Canada, Innovative Medicines Initiative (EU/EFPIA), Janssen, Merck KGaA Darmstadt Germany, MSD, Novartis Pharma AG, Ontario Ministry of Economic Development and Innovation, Pfizer, São Paulo Research Foundation-FAPESP, Takeda, and the Wellcome Trust.

ACKNOWLEDGMENT

We thank Jens Strobach and Katharina Bauer for biological testing. The authors wish to acknowledge CSC – IT Center for Science, Finland, for computational resources.

ABBREVIATIONS

ATP, adenosine triphosphate; R-spine, regulatory spine; TRT, target residence time; NAH, *N*-acylhydrazone; MAP, mitogen activated protein; TNF, tumor necrosis factor; HLM, human liver microsome; MD, molecular dynamics; HR, hydrophobic region.

REFERENCES

(1) Manning, G. The Protein Kinase Complement of the Human Genome. *Science (80-.).* **2002**, *298* (5600), 1912–1934. https://doi.org/10.1126/science.1075762.

(2) Koul, H. K.; Pal, M.; Koul, S. Role of P38 MAP Kinase Signal Transduction in Solid Tumors. *Genes Cancer* **2013**, *4* (9–10), 342–359. https://doi.org/10.1177/1947601913507951.

(3) Igea, A.; Nebreda, A. R. The Stress Kinase P38 as a Target for Cancer Therapy. *Cancer Res.* **2015**, *75* (19), 3997–4002. https://doi.org/10.1158/0008-5472.CAN-15-0173.

(4) García-Cano, J.; Roche, O.; Cimas, F. J.; Pascual-Serra, R.; Ortega-Muelas, M.; Fernández-Aroca, D. M.; Sánchez-Prieto, R.

P38MAPK and Chemotherapy: We Always Need to Hear Both Sides of the Story. *Front. Cell Dev. Biol.* **2016**, *4* (JUN), 1–8. https://doi.org/10.3389/fcell.2016.00069.

(5) Patnaik, A.; Haluska, P.; Tolcher, A. W.; Erlichman, C.; Papadopoulos, K. P.; Lensing, J. L.; Beeram, M.; Molina, J. R.; Rasco, D. W.; Arcos, R. R.; Kelly, C. S.; Wijayawardana, S.R.; Zhang, X.; Stancato, L. F.; Bell, R.; Shi, P.; Kulanthaivel, P.; Pitou, C.; Mulle, L. B.; Farrington, D. L.; Chan, E. M.; Goetz, M. P. A. A First-in-Human Phase I Study of the Oral P38 MAPK Inhibitor, Ralimetinib (LY2228820 Dimesylate), in Patients with Advanced Cancer. *Clin. Cancer Res.* **2016**, *22* (5), 1095–1102. https://doi.org/10.1158/1078-0432.CCR-15-1718.

(6) Bühler, S.; Laufer, S. A. P38 MAPK Inhibitors: A Patent Review (2012 – 2013). *Expert Opin. Ther. Pat.* **2014**, *24* (5), 535–554. https://doi.org/10.1517/13543776.2014.894977.

(7) Fischer, S.; Koeberle, S. C.; Laufer, S. A. P38α Mitogen-Activated Protein Kinase Inhibitors, a Patent Review (2005 – 2011). *Expert Opin. Ther. Pat.* **2011**, *21* (12), 1843–1866. https://doi.org/10.1517/13543776.2011.636737.

(8) Koeberle, S. C.; Romir, J.; Fischer, S.; Koeberle, A.; Schattel, V.; Albrecht, W.; Grütter, C.; Werz, O.; Rauh, D.; Stehle, T.; Laufer, S. Skepinone-L Is a Selective P38 Mitogen-Activated Protein Kinase Inhibitor. *Nat. Chem. Biol.* **2012**, *8* (2), 141–143. https://doi.org/10.1038/nchembio.761.

(9) Koeberle, S. C.; Fischer, S.; Schollmeyer, D.; Schattel, V.; Grütter, C.; Rauh, D.; Laufer, S. A. Design, Synthesis, and Biological Evaluation of Novel Disubstituted Dibenzosuberones as Highly Potent and Selective Inhibitors of P38 Mitogen Activated Protein Kinase. *J. Med. Chem.* **2012**, *55* (12), 5868–5877. https://doi.org/10.1021/jm300327h.

(10) Fitzgerald, C. E.; Patel, S. B.; Becker, J. W.; Cameron, P. M.; Zaller, D.; Pikounis, V. B.; O'Keefe, S. J.; Scapin, G. Structural Basis for P38α MAP Kinase Quinazolinone Andpyridol-Pyrimidine Inhibitor Specificity. *Nat. Struct. Mol. Biol.* **2003**, *10* (9), 764–769. https://doi.org/10.1038/nsb949.

(11) Martz, K. E.; Dorn, A.; Baur, B.; Schattel, V.; Goettert, M. I.; Mayer-Wrangowski, S. C.; Rauh, D.; Laufer, S. A. Targeting the Hinge Glycine Flip and the Activation Loop: Novel Approach to Potent P38α Inhibitors. *J. Med. Chem.* **2012**, *55* (17), 7862–7874. https://doi.org/10.1021/jm300951u.

(12) Fischer, S.; Wentsch, H. K.; Mayer-Wrangowski, S. C.; Zimmermann, M.; Bauer, S. M.; Storch, K.; Niess, R.; Koeberle, S. C.; Grütter, C.; Boeckler, F. M.; Rauh, D.; Laufer, S. Dibenzosuberones as P38 Mitogen-Activated Protein Kinase Inhibitors with Low ATP Competitiveness and Outstanding Whole Blood Activity. *J. Med. Chem.* **2013**, *56* (1), 241–253. https://doi.org/10.1021/jm301539x.

(13) Walter, N. M.; Wentsch, H. K.; Bührmann, M.; Bauer, S. M.; Döring, E.; Mayer-Wrangowski, S.; Sievers-Engler, A.; Willemsen-Seegers, N.; Zaman, G.; Buijsman, R.; Lämmerhofer, M.; Raug, D.; Laufer S. A. Design, Synthesis, and Biological Evaluation of Novel Type I 1 / 2 P38α MAP Kinase Inhibitors with Excellent Selectivity, High Potency, and Prolonged Target Residence Time by Interfering with the R-Spine. *J. Med. Chem.* **2017**, *60* (19), 8027–8054. https://doi.org/10.1021/acs.jmedchem.7b00745.

(14) Wentsch, H. K.; Walter, N. M.; Bührmann, M.; Mayer-Wrangowski, S.; Rauh, D.; Zaman, G. J. R.; Willemsen-Seegers, N.; Buijsman, R. C.; Henning, M.; Dauch, D.; Zender, L.; Laufer, S. Optimized Target Residence Time: Type I1/2 Inhibitors for P38α MAP Kinase with Improved Binding Kinetics through Direct Interaction with the R-Spine. *Angew. Chemie Int. Ed.* **2017**, *56* (19), 5363–5367. https://doi.org/10.1002/anie.201701185.

(15) Kornev, A. P.; Haste, N. M.; Taylor, S. S.; Ten Eyck, L. F. Surface Comparison of Active and Inactive Protein Kinases Identifies a Conserved Activation Mechanism. *Proc. Natl. Acad. Sci.* **2006**, *103* (47), 17783–17788. https://doi.org/10.1073/pnas.0607656103.

(16) Copeland, R. A.; Pompliano, D. L.; Meek, T. D. Drug–Target Residence Time and Its Implications for Lead Optimization. *Nat. Rev. Drug Discov.* **2006**, *5* (9), 730–739. https://doi.org/10.1038/nrd2082.

(17) Braga, R. C.; Tôrres, A. C. B.; Persiano, C. B.; Alves, R. O.; Fraga, C. A. M.; Barreiro, E. J.; de Oliveira, V. Determination of the Cardioactive Prototype LASSBio-294 and Its Metabolites in Dog Plasma by LC–MS/MS: Application for a Pharmacokinetic Study. *J. Pharm. Biomed. Anal.* **2011**, *55* (5), 1024–1030. https://doi.org/10.1016/j.jpba.2011.02.031.

(18) Thota, S.; Rodrigues, D. A.; Pinheiro, P. de S. M.; Lima, L. M.; Fraga, C. A. M.; Barreiro, E. J. N-Acylhydrazones as Drugs. *Bioorg. Med. Chem. Lett.* **2018**, *28* (17), 2797–2806. https://doi.org/10.1016/j.bmcl.2018.07.015.

(19) Młochowski, J.; Giurg, M. New Trends in Chemistry and Application of Aromatic and Related Selenaheterocycles. In *Aromaticity in Heterocyclic Compounds*; Ed. Springer, Berlin, 2008; Vol. 2, pp 1–14. https://doi.org/10.1007/7081_2008_7.

(20) Plano, D.; Karelia, D. N.; Pandey, M. K.; Spallholz, J. E.; Amin, S.; Sharma, A. K. Design, Synthesis, and Biological Evaluation of Novel Selenium (Se-NSAID) Molecules as Anticancer Agents. *J. Med. Chem.* **2016**, *59* (5), 1946–1959. https://doi.org/10.1021/acs.jmedchem.5b01503.

(21) Garnica, P.; Encío, I.; Plano, D.; Palop, J. A.; Sanmartín, C. Combined Acylselenourea–Diselenide Structures: New Potent and Selective Antitumoral Agents as Autophagy Activators. *ACS Med. Chem. Lett.* **2018**, *9* (4), 306–311. https://doi.org/10.1021/acsmedchemlett.7b00482.

(22) Chen, Z.; Li, D.; Xu, N.; Fang, J.; Yu, Y.; Hou, W.; Ruan, H.; Zhu, P.; Ma, R.; Lu, S.; Cao, D.; Wu, R.; Ni, M.; Zhang, W.; Su, W.; Ruan, B. H. Novel 1,3,4-Selenadiazole-Containing Kidney-Type Glutaminase Inhibitors Showed Improved Cellular Uptake and Antitumor Activity. *J. Med. Chem.* **2019**, *62* (2), 589–603. https://doi.org/10.1021/acs.jmedchem.8b01198.

(23) Zegzouti, H.; Zdanovskaia, M.; Hsiao, K.; Goueli, S. A. ADP-Glo: A Bioluminescent and Homogeneous ADP Monitoring Assay for Kinases. *Assay Drug Dev. Technol.* **2009**, *7* (6), 560–572. https://doi.org/10.1089/adt.2009.0222.

(24) Bauer, S. M.; Kubiak, J. M.; Rothbauert, U.; Laufer, S. A. From Enzyme to Whole Blood: Sequential Screening Procedure for Identification and Evaluation of P38 MAPK Inhibitors. In *Kinase Screening and Profiling*; Ed. Humana Press, New York, 2016; pp 123–148.

(25) Sherman, W.; Day, T.; Jacobson, M. P.; Friesner, R. A.; Farid, R. Novel Procedure for Modeling Ligand/Receptor Induced Fit Effects. *J. Med. Chem.* **2006**, *49* (2), 534–553. https://doi.org/10.1021/jm050540c.

(26) Lopes, A.; Miguez, E.; Kümmerle, A.; Rumjanek, V.; Fraga, C.; Barreiro, E. Characterization of Amide Bond Conformers for a Novel Heterocyclic Template of N-Acylhydrazone Derivatives. *Molecules* **2013**, *18* (10), 11683–11704. https://doi.org/10.3390/molecules181011683.

(27) Pinheiro, P. D. S. M.; Rodrigues, D. A.; Alves, M. A.; Tinoco, L. W.; Ferreira, G. B.; de Sant'Anna, C. M. R.; Fraga, C. A. M. Theoretical and Experimental Characterization of 1,4-N···S σ-Hole Intramolecular Interactions in Bioactive N -Acylhydrazone Derivatives. *New J. Chem.* **2018**, *42* (1), 497–505. https://doi.org/10.1039/C7NJ03543H.

(28) Bastos, I. T. S.; Pinheiro, P. de S. M.; Costa, F. N.; Rocha, M. D.; Sant'anna, C. M. R.; Braz, D.; Souza, E. T.; Martins, M. A.; Barreiro, E. J.; Ferreira, F. F.; Barroso, R. C.; Fraga, C. A. M.. Design, Synthesis, Experimental and Theoretical Characterization of a New Multitarget 2-Thienyl-N-Acylhydrazone Derivative. *Pharmaceuticals* **2018**, *11* (4). 1-14 https://doi.org/10.3390/ph11040119.

(29) Treiber, A.; Dansette, P. M.; El Amri, H.; Girault, J.-P.; Ginderow, D.; Mornon, J.-P.; Mansuy, D. Chemical and Biological Oxidation of Thiophene: Preparation and Complete Characterization of Thiophene S -Oxide Dimers and Evidence for Thiophene S -Oxide as an Intermediate in Thiophene Metabolism in Vivo and in Vitro. *J. Am. Chem. Soc.* **1997**, *119* (7), 1565–1571. https://doi.org/10.1021/ja962466g.

(30) Reich, H. J.; Hondal, R. J. Why Nature Chose Selenium. *ACS Chem. Biol.* **2016**, *11* (4), 821–841. https://doi.org/10.1021/acschembio.6b00031.

(31) Wessjohann, L. A.; Schneider, A.; Abbas, M.; Brandt, W. Selenium in Chemistry and Biochemistry in Comparison to Sulfur. *Biol. Chem.* **2007**, *388* (10), 997–1006. https://doi.org/10.1515/BC.2007.138.

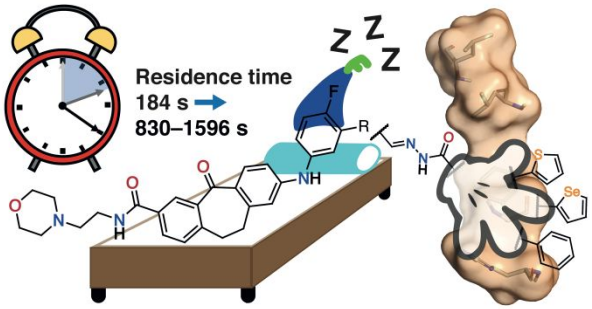
Residence time
184 s
830–1596 s
Z Z Z
F
R
NH
O
N
H
S
Se